Supplemental Figures

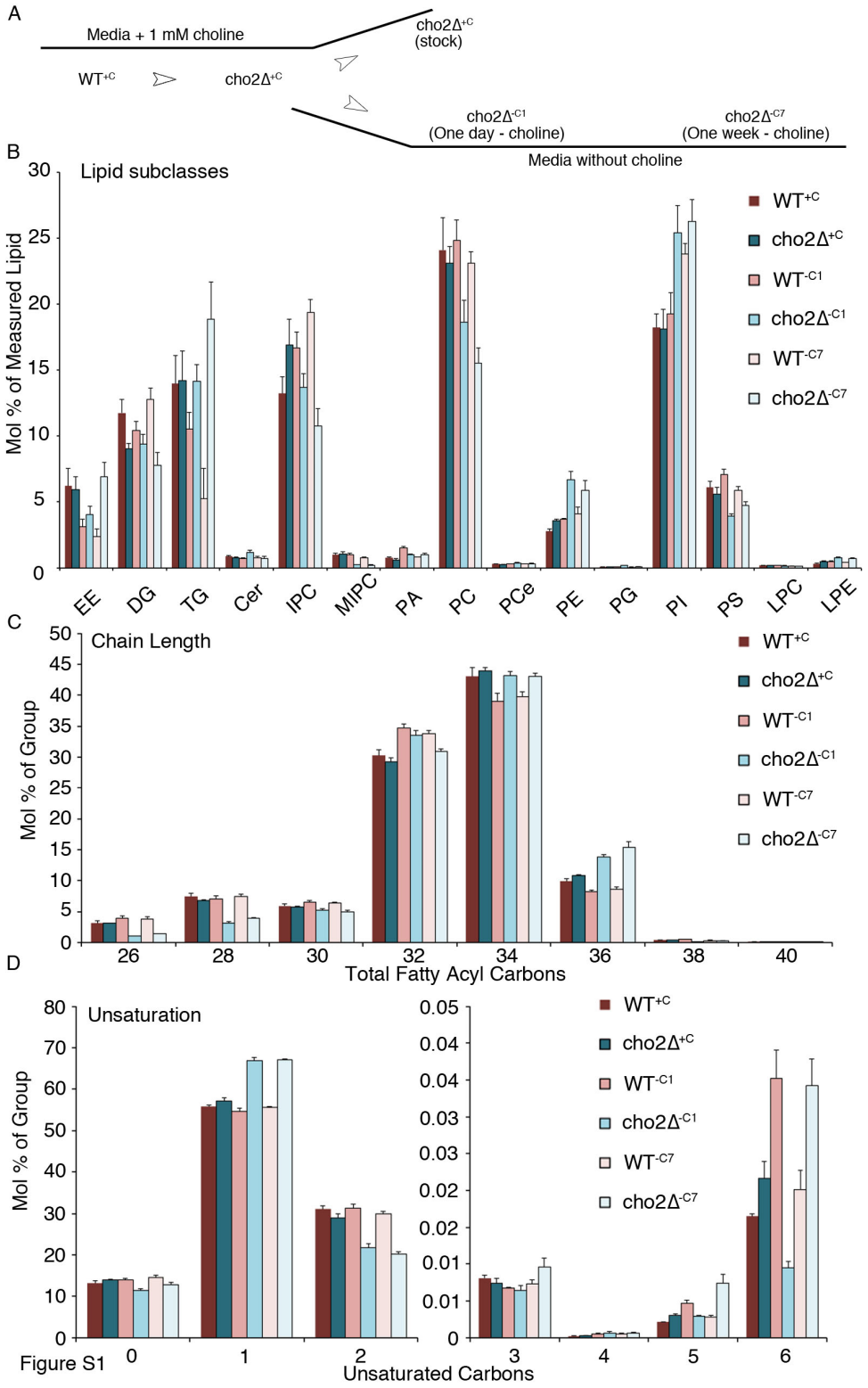

Figure S1

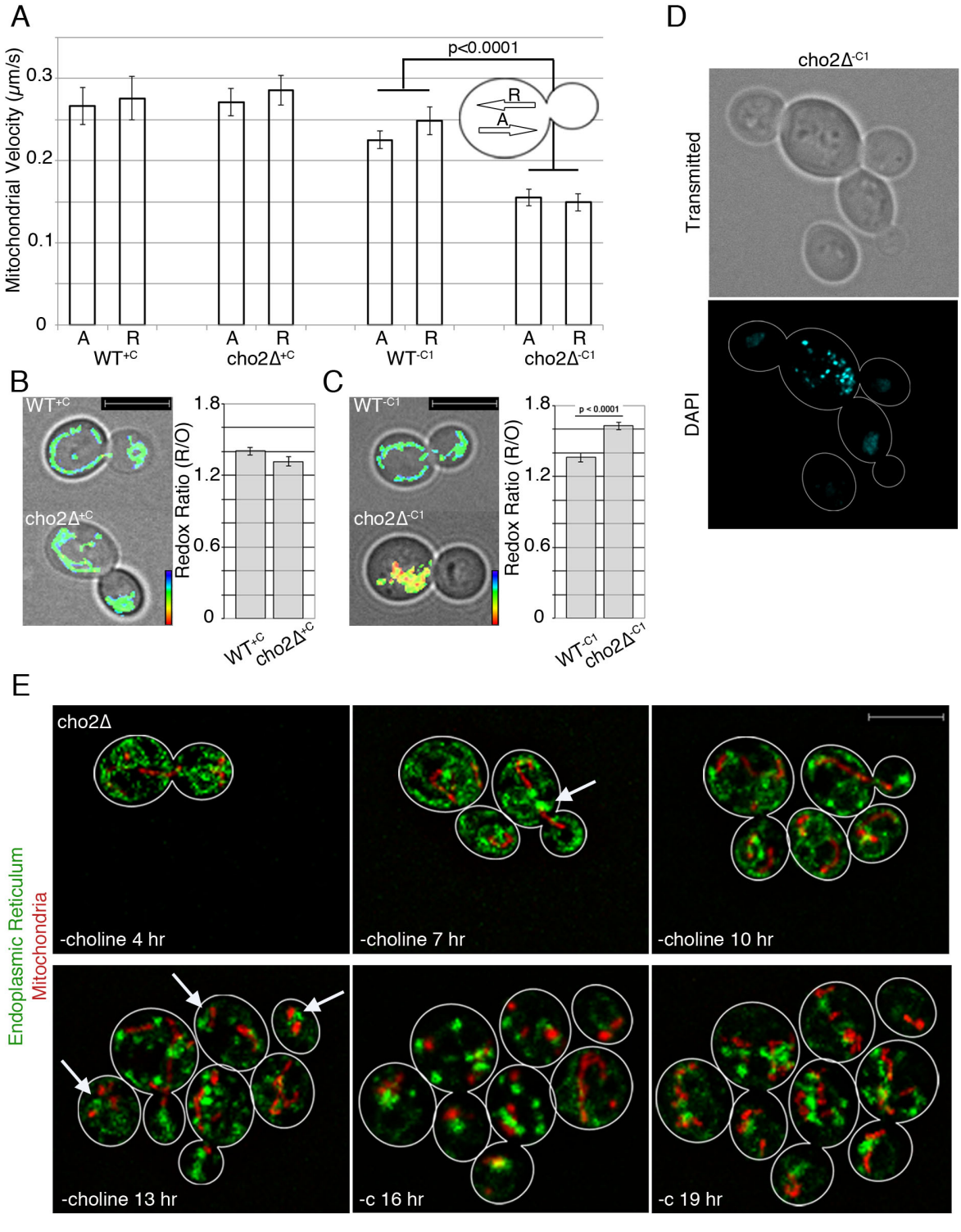
A
Mitochondrial Velocity (μm/s)
0.3
0.2
0.1
0
p<0.0001
R
A
A R
WT+C
cho2Δ+C
WT-C1
cho2Δ-C1
B
WT+C
cho2Δ+C
Redox Ratio (R/O)
1.8
1.2
0.6
0
C
WT-C1
cho2Δ-C1
p < 0.0001
D
cho2Δ-C1
Transmitted
DAPI
E
cho2Δ
Endoplasmic Reticulum
Mitochondria
-choline 4 hr
-choline 7 hr
-choline 10 hr
-choline 13 hr
-c 16 hr
-c 19 hr

Figure S2

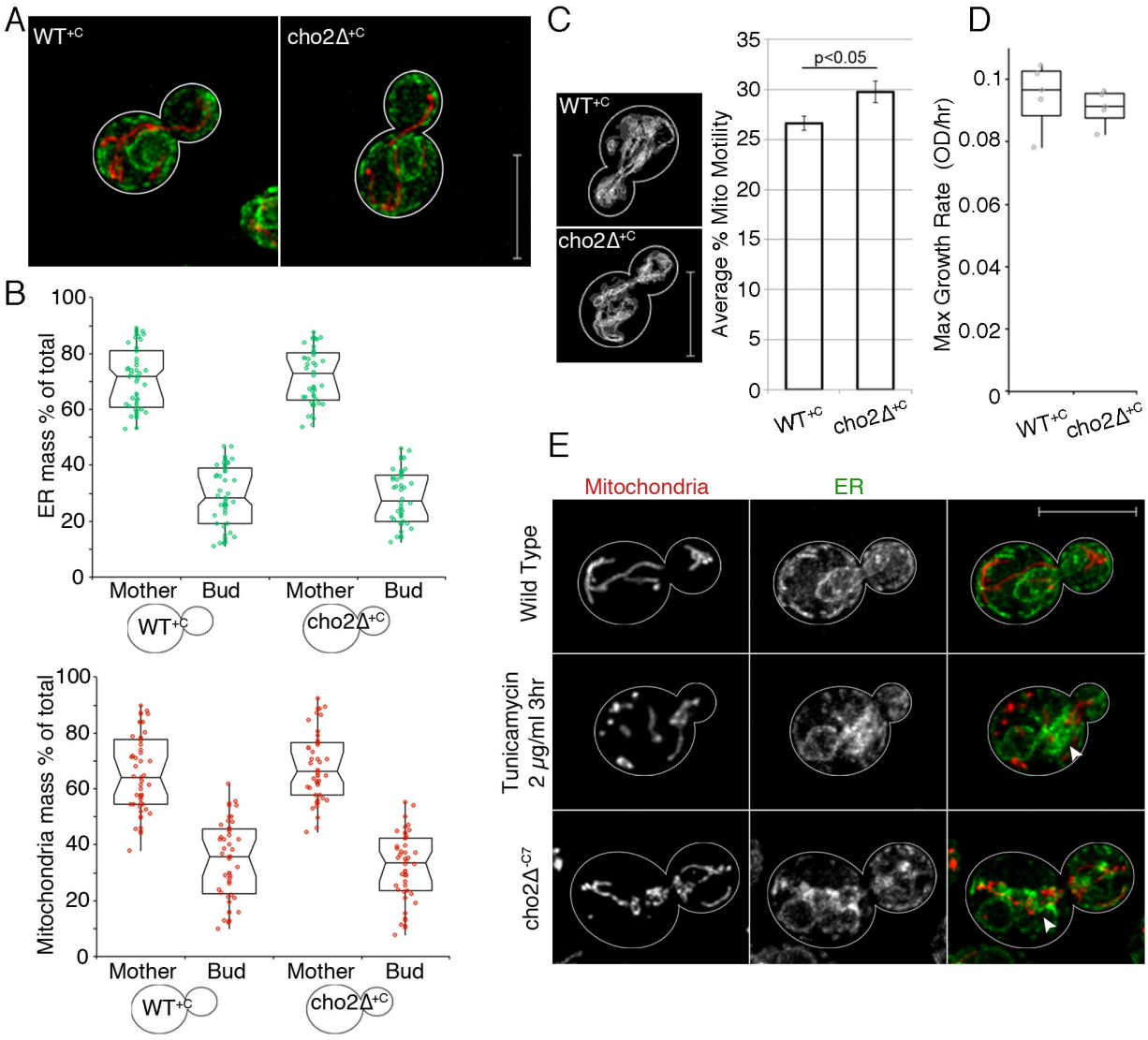
A
WT+C
cho2Δ+C
B
ER mass % of total
Mother
Bud
Mother
Bud
WT+C
cho2Δ+C
Mitochondria mass % of total
Mother
Bud
Mother
Bud
WT+C
cho2Δ+C
C
WT+C
cho2Δ+C
Average % Mito Motility
p<0.05
WT+C
cho2Δ+C
D
Max Growth Rate (OD/hr)
WT+C
cho2Δ+C
E
Mitochondria
ER
Wild Type
Tunicamycin 2 μg/ml 3hr
cho2Δ-C7

Figure S3

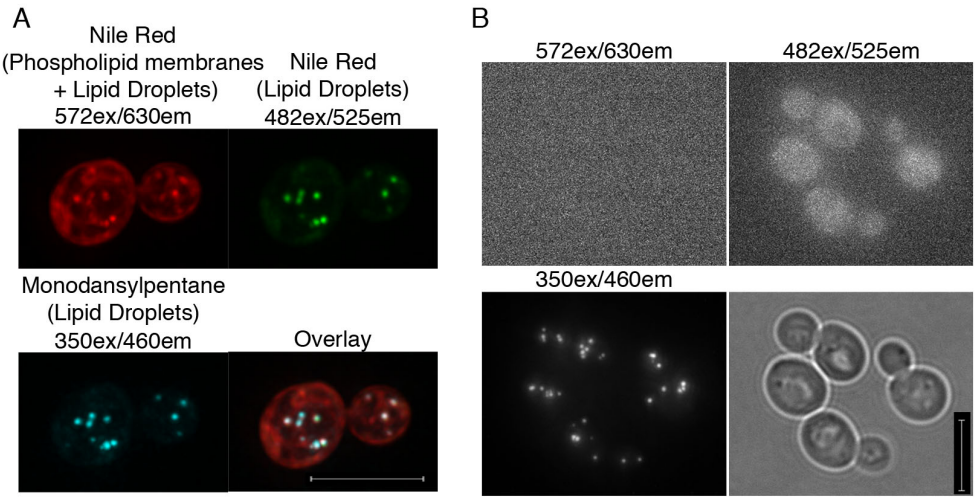
A
Nile Red
(Phospholipid membranes
+ Lipid Droplets)
572ex/630em
Nile Red
(Lipid Droplets)
482ex/525em
Monodansylpentane
(Lipid Droplets)
350ex/460em
Overlay
B
572ex/630em
482ex/525em
350ex/460em

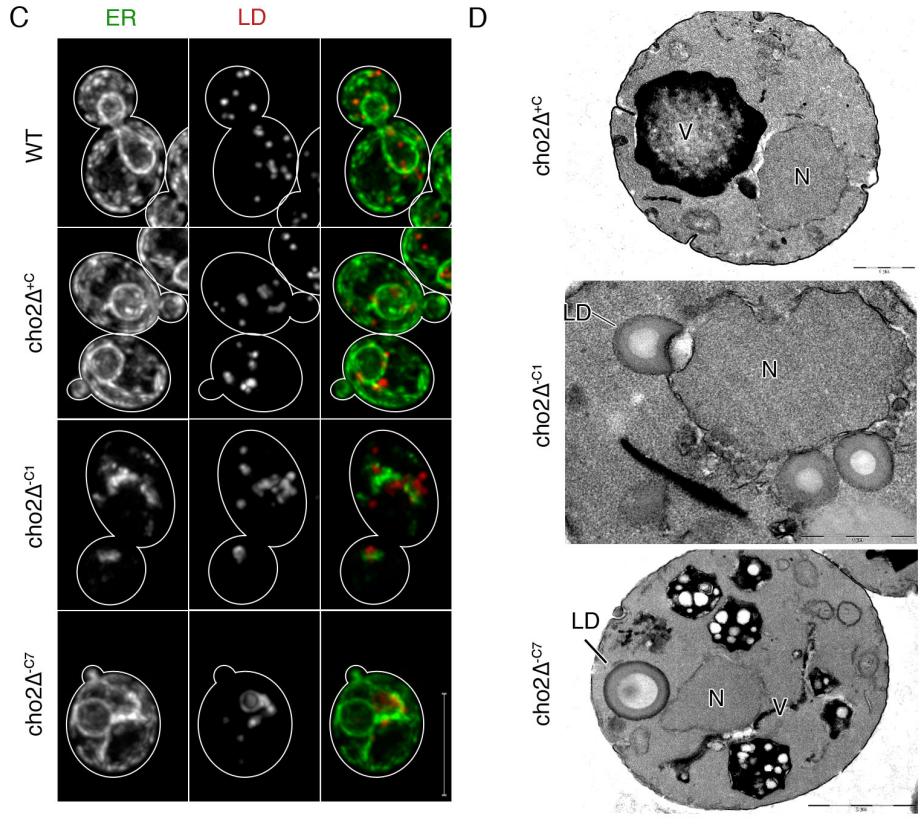
C
ER
LD
WT
cho2Δ+C
cho2Δ-C1
cho2Δ-C7
D
cho2Δ+C
V
N
cho2Δ-C1
LD
N
cho2Δ-C7
LD
N
V

Figure S4

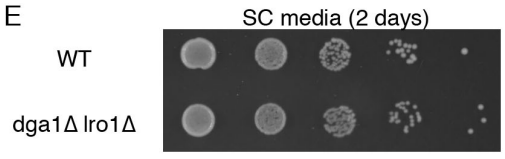
E
SC media (2 days)
WT
dga1Δ lro1Δ

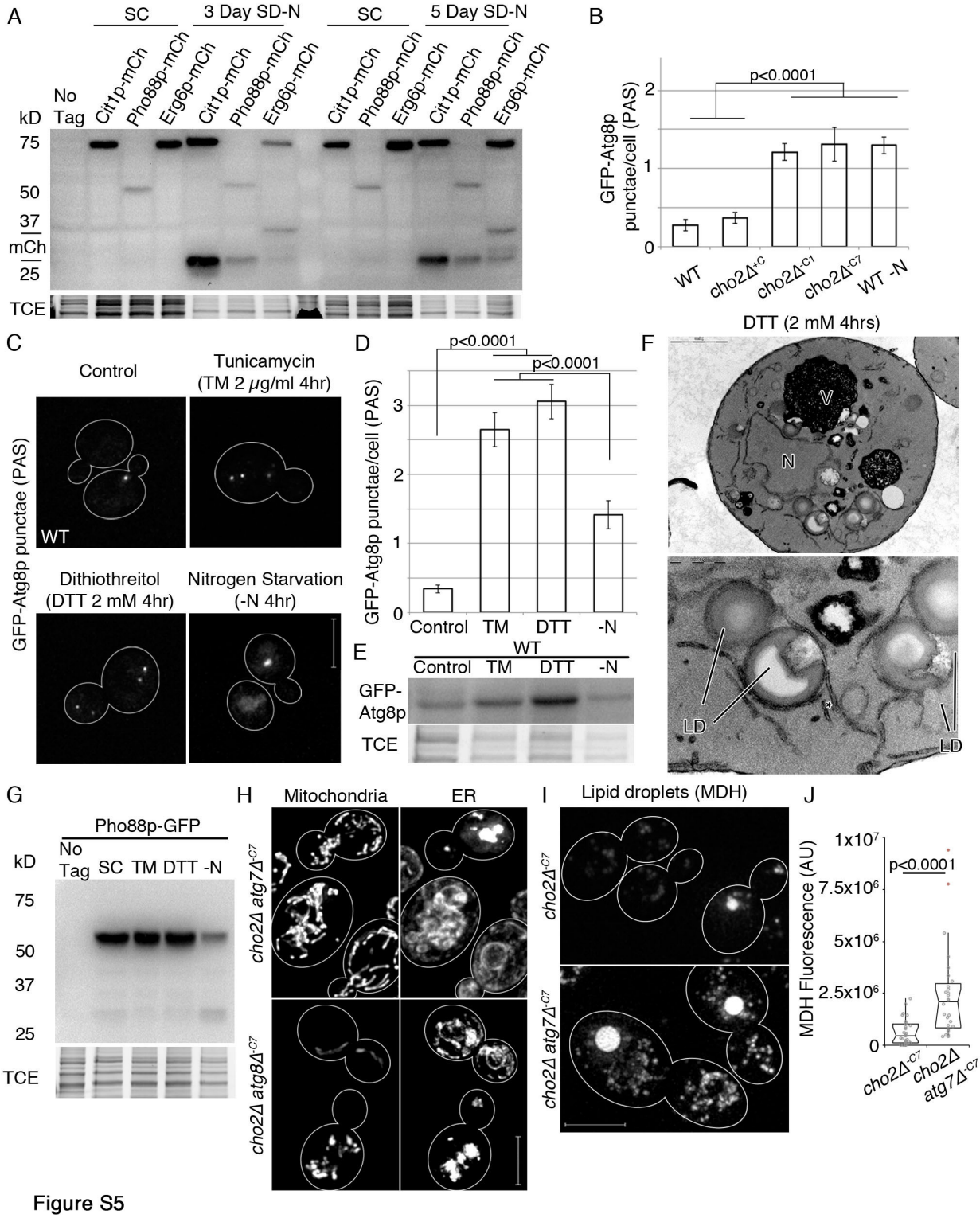
A
SC
3 Day SD-N
SC
5 Day SD-N
No Tag
Cit1p-mCh
Pho88p-mCh
Erg6p-mCh
kD
75
50
37
mCh
25
TCE
B
GFP-Atg8p punctae/cell (PAS)
p<0.0001
WT
cho2Δ+C
cho2Δ-C1
cho2Δ-C7
WT -N
C
Control
Tunicamycin (TM 2 μg/ml 4hr)
Dithiothreitol (DTT 2 mM 4hr)
Nitrogen Starvation (-N 4hr)
GFP-Atg8p punctae (PAS)
WT
D
p<0.0001
p<0.0001
GFP-Atg8p punctae/cell (PAS)
Control
TM
DTT
-N
E
WT
Control
TM
DTT
-N
GFP-Atg8p
TCE
F
DTT (2 mM 4hrs)
V
N
LD
LD
G
Pho88p-GFP
No Tag
SC
TM
DTT
-N
kD
75
50
37
25
TCE
H
Mitochondria
ER
cho2Δ atg7Δ-C7
cho2Δ atg8Δ-C7
I
Lipid droplets (MDH)
cho2Δ-C7
cho2Δ atg7Δ-C7
J
MDH Fluorescence (AU)
1x10^7
7.5x10^6
5x10^6
2.5x10^6
0
p<0.0001
cho2Δ-C7
cho2Δ atg7Δ-C7

Figure S5

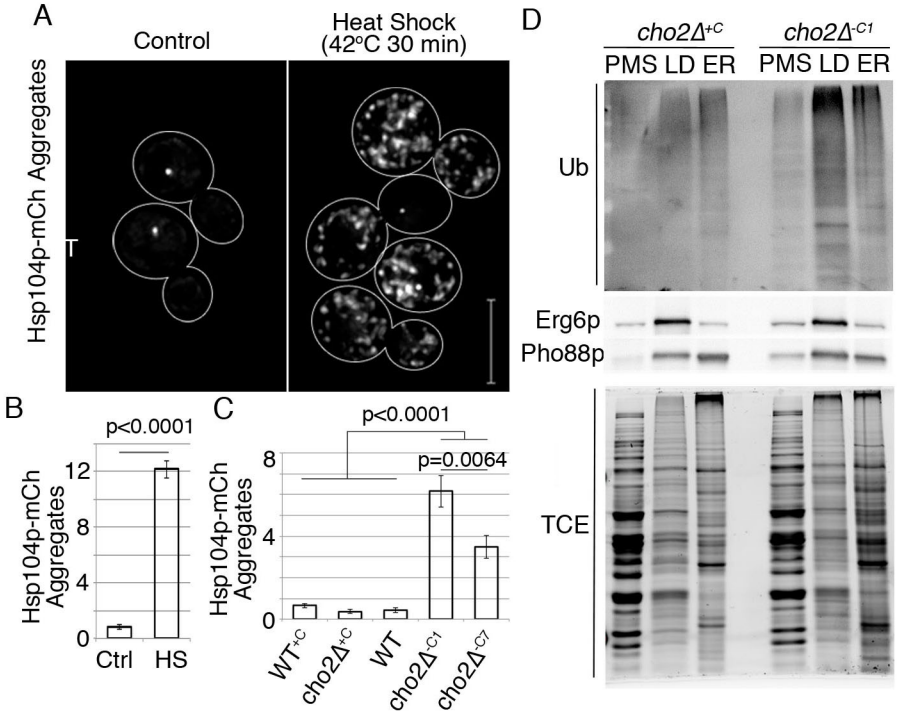
A
Control
Heat Shock
(42°C 30 min)
Hsp104p-mCh Aggregates
B
p<0.0001
Hsp104p-mCh Aggregates
12
8
4
0
Ctrl
HS
C
p<0.0001
p=0.0064
Hsp104p-mCh Aggregates
8
4
0
WT+C
cho2Δ+C
WT
cho2Δ-C1
cho2Δ-C7
D
cho2Δ+C
cho2Δ-C1
PMS LD ER
PMS LD ER
Ub
Erg6p
Pho88p
TCE

Figure S6

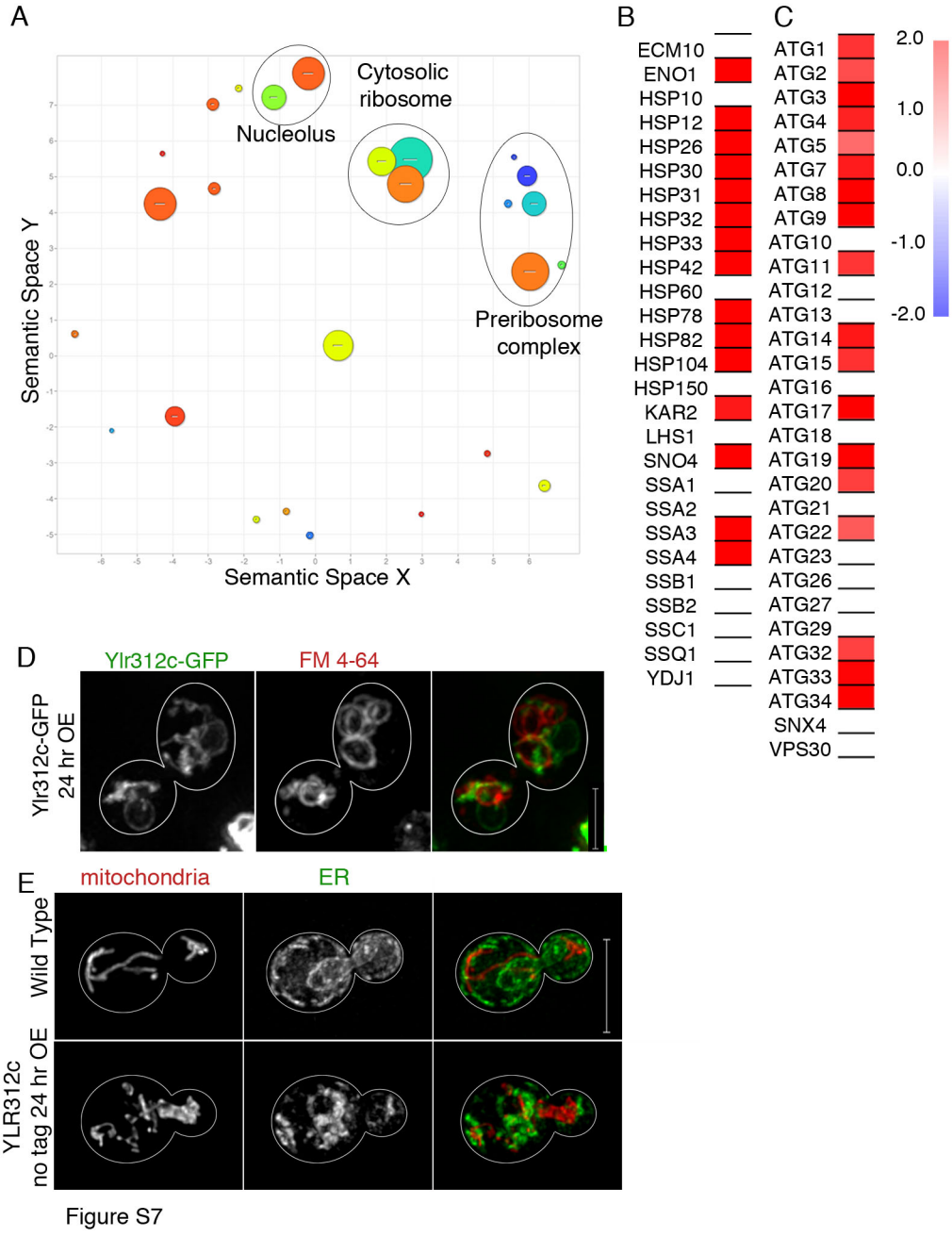
A
Cytosolic ribosome
Nucleolus
Preribosome complex
Semantic Space Y
Semantic Space X
B
ECM10
ENO1
HSP10
HSP12
HSP26
HSP30
HSP31
HSP32
HSP33
HSP42
HSP60
HSP78
HSP82
HSP104
HSP150
KAR2
LHS1
SNO4
SSA1
SSA2
SSA3
SSA4
SSB1
SSB2
SSC1
SSQ1
YDJ1
C
ATG1
ATG2
ATG3
ATG4
ATG5
ATG7
ATG8
ATG9
ATG10
ATG11
ATG12
ATG13
ATG14
ATG15
ATG16
ATG17
ATG18
ATG19
ATG20
ATG21
ATG22
ATG23
ATG26
ATG27
ATG29
ATG32
ATG33
ATG34
SNX4
VPS30
2.0
1.0
0.0
-1.0
-2.0
D
Ylr312c-GFP
FM 4-64
Ylr312c-GFP 24 hr OE
E
mitochondria
ER
Wild Type
YLR312c no tag 24 hr OE

Figure S7

Supplemental Figures Legends

Fig. S1. Effect of acute and chronic defects in PC biosynthesis on phospholipid levels. (a) **Experimental outline followed for lipid imbalance studies.** Wild-type cells were grown in synthetic complete (SC) media supplemented with 1 mM choline (WT^{+C}). The *CHO2* gene was replaced with an auxotrophic marker and selected on appropriate dropout media supplemented with 1 mM choline ($cho2\Delta^{+C}$). These cells were then grown to mid-log phase in SC media containing 1 mM choline and propagated in fresh choline-free SC medium for 1 ($cho2\Delta^{-C1}$) or 7 days ($cho2\Delta^{-C7}$). (b) **Levels of total measured lipid grouped by subclass.** (c) **Levels of side chain length grouped by side chain.** (d) **Levels of unsaturated carbons of all phospholipids grouped by number.** (Related to Figure 1.)

Fig. S2. The effect of acute lipid imbalance on mitochondria redox state and motility.
(a) Mitochondrial motility is decreased in *cho2*Δ cells under acute lipid stress. The velocity of anterograde (A) and retrograde mitochondrial movement was measured as described in previously (Swayne et al., 2011). (b-c) **Mitochondria are more reduced during acute lipid imbalance.** Representative fluorescent images of WT and *cho2*Δ cells grown to mid-log phase with (b) and without (c) choline. Mitochondrial matrix redox state was probed using mitochondria-targeted redox-sensitive GFP (mit-roGFP$_1$). The bar graph shows the average cellular mitochondrial redox ratio of reduced to oxidized mito-roGFP (mean +/- SEM). *P*-values were calculated using the Student's *t*-test. One representative trial is shown from 3 independent trials, n>30 for each trial. Images shown are maximum projections of 3-D Z-stacks. Bar: 5 µm. (d) ***cho2*Δ^{-C1} cells become multi-budded.** Example of a multi-budded *cho2*Δ cell counterstained with DAPI to show cellular and mitochondrial DNA (blue). Nuclear DNA is clearly visible in each bud while mtDNA is restricted to the mother cell. The image is maximum projection of 3-D z-stacks. Bar: 5 µm. (e) **The velocity of mitochondrial movement decreases during acute lipid stress.** Mitochondrial movement was assessed by 4D imaging (3D reconstruction combined with time-lapse imaging) in *cho2*Δ cells that express Cit1p-mCherry and were exposed to acute lipid stress. Z-stacks were obtained at 1 sec intervals. Directed movement was defined as those that were linear over 3 consecutive still frames during the time-lapse series. The bar graph shows the average velocity of mitochondria movement (mean +/- SEM). *P*-values were calculated using the Student's *t*-test. One representative trial is shown from 2 independent trials, n>30 for each trial. The number of directed movements also decreased, three times as many cells had to be assayed for mitochondrial movement in the *cho2*Δ^{-C1} condition. (Related to Figures 2 and 3.)

Fig. S3. Mitochondria and ER are normal in wild-type cells and in *cho2*Δ cells propagated in the presence of choline. (a) **Mitochondria and ER have wild-type morphology with choline supplementation.** Representative fluorescent images of mitochondria and ER, visualized with Cit1p-mCherry (red) and Pho88p-GFP (green) respectively. Images are maximum projections from deconvolved wide-field z-series of WT and *cho2*Δ cells grown in the presence of 1 mM choline. Bar: 5 µm. (b) **Mitochondria and ER have wild-type distribution with choline supplementation.** Distribution data was obtained and quantified as in Figure 3b. One representative trial is shown from 3 independent trials, and n>40 cells for each condition. (c) **Mitochondrial motility is normal with choline supplementation.** Representative images of total motility (grey). Bar: 5 µm. Mitochondrial motility was assayed as in Figure 3c. One representative trial is shown from 3 independent trials, and n>20 for each condition. *P*-values were determined using the Student's *t*-test. (d) **Cell growth rates are at wild-type levels with choline supplementation.** Box plot representing maximum growth rates of strains grown in SC with choline supplementation. Data obtained as in Figure 3d. One representative trial is shown from 3 independent trials, and n=5. (e) **Mitochondria and ER morphology during prolonged lipid stress is similar to UPR-induced stress.** Representative fluorescent maximum projections of untreated wild-type cells (WT), wild-type cells treated with TM and *cho2*Δ cells under chronic lipid imbalance (*cho2*Δ^{-C7}). Mitochondria and ER are visualized using Cit1p-mCherry (red) and Pho88p-GFP (green). Arrowheads point to ER/mitochondrial aggregates seen during UPR-induced stress and lipid stress. Bar: 5 µm. (Related to Figures 2 and 3.)

Fig. S4. LDs accumulate during lipid imbalance. (a) **MDH labels LDs in yeast.** Representative fluorescent images of WT cells grown to mid-log phase in SC media and stained with Nile red (red and green) and MDH (cyan). Nile red stains all cellular lipids and LDs. However, the wavelength of its emitted fluorescence varies depending on the structures stained. Red: total cellular lipids. Green: Lipid droplets. MDH labeling co-localizes with Nile Red-stained LDs. Images are maximum projections from deconvolved wide-field z-series. Bar: 5 µm. MDH staining is bright and photostable. (b) It also has no obvious bleed-through to red and green channels and is therefore compatible with fluorophores including GFP and mCherry. (c) **Additional examples of *cho2*Δ cells during lipid**

imbalance. Representative TEM images of *cho2*Δ cells propagated in the presence of choline (*cho2*Δ^{+}) or in the absence of choline for 1 (*cho2*Δ^{-C1}) or 7 (*cho2*Δ^{-C7}) days. Bars: *cho2*Δ^{+} and *cho2*Δ^{-C1}: 1 µm; *cho2*Δ^{-C7}: 2 µm. N: nucleus. LD: lipid droplet. V: vacuole. (d) **LDs and ER are in close proximity to each other during lipid imbalance.** Representative images of ER and LDs in cells expressing Pho88p-GFP (green) and Erg6p-mCherry (red) during lipid imbalance. WT, *cho2*Δ^{+}, *cho2*Δ^{-C1}, and *cho2*Δ^{-C7} cells grown in SC media with and without choline. Images are maximum projections from deconvolved wide-field z-series. Bar: 5µm. (e) **LD biogenesis is not critical in cells that are not exposed to lipid stress.** Dot assay of serially diluted (1:10) WT and *dga1*Δ *lro1*Δ strains on SC media without choline. Strains were grown to mid-log phase in SC media in the presence of choline prior to plating. Strains are shown after 2 days of growth at 30^{o}C. (Related to Figure 4.)

Fig. S5. (a) **Mitochondria, ER, and LDs are delivered to the vacuole during starvation.** Wild-type or *cho2*Δ cells expressing Cit1p-mCherry (a mitochondrial marker), Pho88p-mCherry (an ER marker) or Erg6-mCherry (an LD marker) were constructed. Cells were propagated in SC media or under nitrogen starvation conditions for 3 or 5 days. Protein lysate corresponding to 0.1 OD_{600} of cell culture were analyzed by western blot analysis using an antibody that recognizes mCherry and TCE as a load control. A representative trial is shown from 3 independent trials. (b) **PAS structures increase during lipid imbalance.** Quantification of GFP-Atg8p punctae (PAS and autophagosomes) number per budded cell during control, lipid imbalance, and nitrogen starvation conditions. The data are presented as bar graphs of the mean PAS structure per budded cell +/- SEM P-values were obtained from student's t-test. One representative trial is shown from three independent trials, n>30 for each condition. (c) **PAS structures increase during ER stress.** Representative fluorescent images GFP-Atg8p in WT cells treated with DMSO (control), TM, DTT, or nitrogen starvation for 4 hrs (WT-N). Images are maximum projections from deconvolved wide-field z-series. Bar: 5µm. (d) Quantification of the number of GFP-Atg8p punctae (PAS and autophagosomes) per budded cell in cells described in panel f. The data are presented as bar graphs of the mean PAS number per budded cell +/- SEM P-values were obtained from the Student's t-test. A representative trial is shown from 3 independent trials, n>30 for each condition. (e) **Atg8p expression is increased during ER stress.** Western blots of GFP-Atg8p and TCE as load control. Cells and culture conditions were as in (c-d). Protein lysate corresponding to 0.1 OD_{600} of cell culture was loaded in each lane. A representative trial is shown from 3 independent trials. (f) **Ultrastructural analysis of LDs during ER stress.** Transmission electron micrographs of a DTT treated cell. N: nucleus. LD: lipid droplet. V: Vacuole. The asterisk marks abnormal membrane aggregates in a magnified region of a cell Bar: 500 nm. (g) **ER is not degraded during ER stress.** WT cells expressing Pho88p-GFP (ER) were grown to mid log phase in SC media. Cells were then treated with DMSO, 2µg/mL TM, 2mM DTT or nitrogen starvation for 4 hrs (SD-N). Protein lysate corresponding to 0.01 OD_{600} of cell culture were analyzed using Western blots and antibodies that recognize GFP. Representative trial is shown from 3 independent experiments. (h) **Macroautophagy is required for adaptation to the lipid imbalance produced by defects in PC biosynthesis.** *cho2*Δ, *cho2*Δ *atg7*Δ or *cho2*Δ *atg8*Δ cells were propagated in choline-free media for 7 days. Wild-type cells (WT) propagated in SC media were used as a control. Maximum projections of illustrating severe defects in the morphology of ER (Pho88p-GFP; green) and mitochondria (Cit1p-mCherry; red) of *cho2*Δ *atg7*Δ or *cho2*Δ *atg8*Δ cells under chronic lipid stress. Bar: 5µm. (i-j) **LDs accumulate during chronic lipid imbalance in autophagy mutants.** (i) Maximum projections of MDH-stained LDs in *cho2*Δ and *cho2*Δ atg7Δ cells propagated in choline-free media for 7 days. Bar: 5 µm. (j) Quantitation of MDH-stained LD fluorescence of cells described panel b. Data is represented using skeletal notched dot box plots showing medians, quartiles, and outliers. P-values were calculated using the non-parametric Mann-Whitney test. A representative trial is shown from 3 independent trials, n>25 for each condition. (Related to Figure 5.)

Fig. S6. Characterization of heat-shock aggregates and LDs that form in yeast under stress conditions. (a-b) **Hsp104p protein aggregates increase drastically during heat shock.** Representative fluorescent images showing Hsp104p-mCh labeled protein aggregates in otherwise WT cells before and after 30 minute heat shock at 42 degrees Celsius. Images are maximum projections from deconvolved wide-field z-series. Bar: 5µm. (b) Quantification of the number of Hsp104p-mCh aggregate number per budded cell during conditions described in d. The data are presented as bar graphs of the mean protein aggregate number per budded cell +/- SEM P-values were obtained from the Student's t-test. A representative trial is shown from 3 independent trials, n>30 for each condition. (c) **Protein aggregates increase during lipid imbalance.** Quantification of Hsp104p-mCh aggregate number per budded cell during conditions described in Fig 4d. The data are presented as bar graphs of the mean Hsp104-mCh aggregate per budded cell +/- SEM P-values were obtained from student's t-test. One representative trial is shown from three independent trials, n>30 for each condition. (d) **Poly-ubiquitinated proteins are enriched in LDs over bulk ER**

during lipid imbalance in *cho2Δ*$^{-Cl}$ cells. Strains were grown as previously described in Fig 1. Lipid droplets (LD) and bulk ER were isolated from mid-log phase *cho2*Δ yeast that were not stressed (*cho2*Δ^{+Cl}) or exposed to acute lipid stress (*cho2*Δ^{C-l}) as described in methods. Post mitochondrial supernatant (PMS), LD, and ER fractions were subjected to western blot analysis. Erg6-mCh was used as a marker for LD while Pho88-GFP was used as a maker for ER to assess purity of LD and ER fractions along with TCE staining profile. The blots shown are representative of 3 independent trials. (Related to Figure 6.)

Fig. S7. RNAseq reveals numerous stress responses activated upon glycerophospholipid imbalance (a) **Down regulated RNA transcripts during lipid stress are related to protein synthesis. Revigo plot of GO terms that are down-regulated during acute lipid stress.** Data was analyzed as described in Figure 5. (b) **Heat shock and protein chaperone related transcripts are up regulated during lipid imbalance.** Heatmap showing $\log_2$ fold change of autophagy-related transcripts. (c) **Autophagy related transcripts are up regulated during lipid imbalance.** Heatmap showing $\log_2$ fold change of autophagy-related transcripts. (d) **Additional example**, as in Fig. 7e. (e) **Overexpression of YLR312c results in defects in the morphology of mitochondria and ER.** Representative images of WT cells (WT is same as Fig. S3e) expressing Pho88p-GFP (ER) and Cit1p-mCh (mitochondria) along with either a vector or GAL1-Ylr312p (untagged) OE construct grown on 2% galactose for 24 hours. Images are max projections from deconvolved wide-field z-series. Bar: 5 µm. Bar: 5 µm. (Related to Figure 7.)

Table S1. RNAseq reveals numerous stress responses activated upon glycerophospholipid imbalance. RNAseq data of differentially expressed mRNAs between WT and *cho2*Δ^{-Cl} cells. Columns A through M are described as follows. Column A lists the systematic yeast ORF name. Column B lists the standard gene name, while C denotes the chromosomal locus. Column D and E are WT and *cho2*Δ^{-Cl} labels. Column F describes the statistical test status. Column G and H list the FPKM of WT and *cho2*Δ^{-Cl} cells respectively. The change in mRNA levels is expressed as the base 2 log of the fold change. Column K lists the uncorrected p-value. Column L lists the FDR-adjusted p-value test statistic. Column M states outcome of significance after Benjamini-Hochberg correction for multiple testing. (Related to Figure 7.)

Supplemental Movie Legends

Smov. 1. ER morphology defects appear prior to mitochondrial defects during acute lipid imbalance. WT and *cho2*Δ cells were grown to mid-log phase in choline-containing media, immobilized in a microfluidic chamber and perfused with choline-free SC media. Time-lapse images of Cit1p-mCherry-labeled mitochondria (red) and Pho88p-GFP-labeled ER (green) in WT and *cho2*Δ cells were obtained every 30 min for 24 hr. WT is shown first, *cho2*Δ cells are shown second in concatenated movie. Movie shown is representative time-lapse images are maximum projections of deconvolved wide-field z-series. (Related to Figure 2.)

Smov. 2. LDs form at sites of ER aggregation. WT and *cho2*Δ cells were grown to mid-log phase in choline-containing media, immobilized in a microfluidic chamber and perfused with choline-free SC media. Time-lapse images of Erg6p-mCherry-labeled LD (red) and Pho88p-GFP-labeled ER (green) in WT and *cho2*Δ cells were obtained every 30 min for 24 hr. WT is shown first, *cho2*Δ cells are shown second in concatenated movie. Movie shown is representative time-lapse images are maximum projections of deconvolved wide-field z-series. (Related to Figure 4.)

Supplemental Experimental Procedures

Yeast strains and growth conditions

All *S. cerevisiae* strains used in this study are derivatives of the wild-type BY4741 strain (*MAT***a** *his3Δ1 leu2Δ0 met15Δ0 ura3Δ0*) and described in Supplemental Table 3. All gene knockouts were created using primers described in Supplemental Table 1. The primers were modified to use the pOM tagging series as a deletion set, allowing the use of cre/lox for removal of auxotrophic markers after genes of interest were deleted (Gauss et al., 2005). GFP and mCherry fusions were constructed using modules from the pFA6a series (Longtine et al., 1998) and pCY series (Young et al., 2012), respectively. Strains were selected using dropout media or addition of antibiotics (200 µg/ml G418, 300 µg/ml Hygromycin B), as needed.

Growth rates

Growth curves were measured using an automated plate reader (Tecan; Infinite M200, Research Triangle Park, NC). Each strain was grown to mid-log phase in SC with 1 mM choline and diluted to an OD_{600} of 0.07 (2.0 x 10^6 cells/ml). 10 µl of each of the diluted strains was added wells containing 200 µl SC in a 96-well plate. Cells were propagated at 30 °C, and optical density measurements (OD_{600}) were made every 20 min for 72 hrs. Each strain was plated in quintuplicate and the growth curves averaged or maximum growth rate (slope) calculated using the greatest change in OD_{600} over a 240 min interval in 72 hrs. Growth rates were estimated using linear regression.

Lipid Droplet Stains

Mid-log phase growing yeast were stained with 50 µM monodansylpentane (MDH) (Abgent Biotech, San Diego, CA) for 15 min at RT in SC media. Cells were then concentrated for immediate imaging. Mid-log phase growing yeast were stained with 0.5 µg/mL Nile Red for 15 min at RT in SC media. Cells were washed 3 times and concentrated immediately before imaging.

Western Blots

Western blot analysis was performed using standard procedures on PVDF (Immobilon-FL; EMD Millipore, Billerica MA). Briefly, total protein was collected from 0.5 OD_{600} of relevant cultures in 150 µL lysis buffer containing 50 mM imidazole pH 7.4, 10 mM EDTA, 1% triton X-100, 2 mM PMSF, and protease inhibitor cocktails (pepstatin A, chymostatin, antipain, leupeptin, aprotinin, benzamidine, and phenanthroline). Samples were vortexed with 100 µL of glass beads for 5 min. Samples were then incubated at 100 ^{o}C for 5 min with the addition of 50 µL SSB (SDS Sample Buffer). For protein detection, 40 µL of protein lysate was loaded onto a 10% SDS-PAGE gel. Before the transfer of proteins, the gel was incubated with (4.5:4.5:1) mix of water:methanol:trichloroethanol) (TCE) for 5 min. After SDS PAGE, the TCE was activated to crosslink to proteins in the gel by exposure to UV light (300 nm) for 2.5 min. Cross-linked proteins were detected by 2.0 sec exposure to 300 nm illumination, and used as a protein load control (Ladner et al., 2004). The gel was then transferred to a PVDF membrane. After transfer, the PVDF membrane was rinsed and dried for 1 hr prior blocking, and incubation with primary and secondary antibodies. Primary antibodies used include mouse monoclonal anti-GFP (Roche, Indianapolis, IN; #11 814 460 001), mouse monoclonal anti-mCherry (Abcam, Cambridge, MA; #ab125096), and rat monoclonal anti-tubulin YOL 1/34 (Abcam, Cambridge, MA; #ab6161). Western blots were imaged using Luminata Forte Western HRP substrate (EMD Millipore, Billerica, MA) and the BIORAD Chemidoc MP imaging system (BIORAD, Hercules, CA)

Electron Microscopy

Electron Microscopy was used to visualize the ultra structure of cells. We used a glutaraldehyde fixation with osmium-thiocarbohydrazide-osmium staining procedure as described previously (Perkins and McCaffery, 2007). Briefly, 50 OD_{600} were collected for analysis, all strains were grown to approximately 0.5 OD_{600} in SC media, WT, WT +2 mM DTT, *cho2*Δ^{+C}, *cho2*Δ^{-C1}, and *cho2*Δ^{-C7} at 30 ^{O}C with 225 rpm shaking. Cultures were collected, resuspended in fixation buffer (3% glutaraldehyde, 0.1 M Na-Cacodylate pH 7.4, 5 mM $CaCl_2$, 5 mM $MgCl_2$, 2.5% sucrose) and fixed for 1 hour at 25 ^{O}C with gentle agitation. Cells were washed with 100 mM Cacodylate pH 7.4, then buffer TDES. Cells were resuspended in TDES and incubated at RT for 10 min, washed with 1 ml 0.1 M phosphocitrate/1 M sorbitol and incubated with zymolyase solution (0.5 ml phosphocitrate/sorbitol, 50 µl B-glucuronidase, 25 µl of 10 mg/ml zymolyase. Cultures were incubated in this solution for 30 min at 30^{O}C with gentle agitation. Cultures were then washed with 0.1 M cacodylate/5 mM $CaCl_2$/1 M sorbitol and embedded in 2% low temperature agarose. Blocks were then post fixed with 1%OsO_4/1% K ferrocyanide in 0.1M cacodylate/5mM $CaCl_2$, pH 6.8 and incubated at RT for 30 min. Blocks were washed 4x in ddH_2O and transferred to

1% thiocarbohydrazide at RT for 5 min, then washed 4x with ddH_2O. Blocks were then stained with Kellenberger's Uranyl Acetate overnight. Cultures were dehydrated through a graded series of ethanol (50% to 100% on ice), and transferred to 1:1 ethanol/propylene oxide for 10 min, and 100% propylene oxide 2 x 5 min. Blocks were then transferred to 1:1 propylene oxide/Spurr resin for overnight incubation under vacuum. Blocks were then transferred to fresh Spurr resin for 4-6 hours before being transferred to beem capsules and polymerize in fresh Spurr resin overnight, section, and post stained with lead and uranyl acetate.

RNA Sequencing

RNA was extracted from mid-log phase yeast cells using the RNeasy kit (Qiagen, Germantown, MD). RNA was analyzed for degradation and RNA Integrity Number scores were satisfactory (RIN>9). RNA-seq was performed on an Illumina HiSeq2000 generating 200m 100 bp Single End reads per lane, with 10 samples multiplexed per lane (average 20m raw reads per sample) by the Columbia Genome Center. Data was analyzed using Tophat and Cufflinks protocol as described (Trapnell et al., 2012). Differentially expressed genes were then analyzed using DAVID functional annotation tool (Huang et al., 2009) to group the large sets of up-regulated and down-regulated genes into gene ontology (GO) terms, and REVIGO (Supek et al., 2011) to remove redundant GO terms and group-related GO terms in semantic similarity-based scatterplots.

Lipidomics

Yeast lipid extracts were prepared using a modified Bligh/Dyer procedure (Bligh and Dyer, 1959), spiked with appropriate internal standards, and analyzed using a 6490 Triple Quadrupole LC/MS system (Agilent Technologies, Santa Clara, CA). Glycerophospholipids and sphingolipids were separated with normal-phase HPLC as described before (Chan et al, 2012), with a few changes. An Agilent Zorbax Rx-Sil column (inner diameter 2.1 x 100 mm) was used under the following conditions: mobile phase A (chloroform:methanol:1 M ammonium hydroxide, 89.9:10:0.1, v/v) and mobile phase B (chloroform:methanol:water:ammonium hydroxide, 55:39.9:5:0.1, v/v); 95% A for 2 min, linear gradient to 30% A over 18 min and held for 3 min, and linear gradient to 95% A over 2 min and held for 6 min. Sterols and glycerolipids were separated with reverse-phase HPLC using an isocratic mobile phase as before (Chan et al, 2012) except with an Agilent Zorbax Eclipse XDB-C18 column (4.6 x 100 mm).

Quantification of lipid species was accomplished using multiple reaction monitoring (MRM) transitions (Chan et al, 2012; Guan et al 2010) in conjunction with referencing of appropriate internal standards: PA 17:0/14:1, PC 17:0/20:4, PE 17:0/14:1, PG 17:0/20:4, PI 17:0/20:4, PS 17:0/14:1, LPC 17:0, LPE 14:0, Cer d18:0/17:0, D_7-cholesterol, cholesteryl ester (CE) 17:0, 4ME 16:0 diether DG, and D_5-TG 16:0/18:0/16:0 (Avanti Polar Lipids, Alabaster, AL).

Lipid Droplet and Endoplasmic Reticulum Isolation

Lipid droplets were isolated according to the procedure developed by G. Daum (Schmidt et al., 2013). Briefly, yeast were grown to mid-log phase (0.5 OD/ml), concentrated by centrifugation (4,500 x g for 5 min), washed with water and incubated in spheroplasting buffer A (SP-A; 0.1 M Tris/$S0_4$, pH 9.4) and 1.54 mg DTT/mL SP-A for 10 min at 30°C. Cells were then resuspended in spheroplasting buffer B (SP-B; 1.2 M sorbitol, 20 mM KH_2PO_4, pH 7.4). Spheroplasts were generated by enzymatic digestion with zymolyase-20T (Seikaguku Corporation) at a concentration of 2 mg/g cell wet weight in 6 mL SP-B/g cell wet weight for 1 hr at 30°C. Cells were concentrated by centrifugation, washed twice with SP-B, resuspended in douncing buffer (LD-A; 12% Ficoll 400 in 10 mM MES/Tris pH 6.9, 0.2 mM EDTA) containing 1 mM PMSF and homogenized using a Dounce homogenizer with a loose pestle (30 strokes at 4°C). The homogenate was subjected to centrifugation (7,000 rpm for 5 min at 4°C), and the resulting pellet was resuspended in LD-A and subjected to another round of homogenization. The supernatants form both rounds of homogenization were transferred to an ultracentrifuge tube, overlayered with LD-A and subjected to ultracentrifugation (100,000 x g for 45 min at 4°C). The crude LD (top layer) was subjected to two additional rounds of homogenization (8 strokes) and ultracentrifugation (28,000 rpm for 30 min at 4°C).

An ER-enriched fraction were isolated according to (Wuestehube and Schekman, 1992). Briefly, spheroplasts generated as described above were washed twice with cold 0.7 M sorbitol, 20 mM HEPES, pH 7.4 and resuspended in homogenization buffer JR (0.2 M sorbitol, 50 mM KOAc, 2 mM EDTA, 20 mM HEPES, pH 7.4, 2 mM DTT, 2 mM PMSF and protease inhibitor cocktail). Cells were homogenized using a glass Dounce homogenizer with a loose pestle (30 strokes at 4°C) and the homogenate was subjected to centrifugation (3,000 rpm for 5 min at 4°C Sorvall SS34) and the resulting supernatant was collected and subjected to another round of centrifugation (15,000 rpm for 5 min at 4°C Sorvall SS34). The membrane pellet was resuspended on B88 buffer (20mM HEPES, pH 6.8, 250mM sorbitol, 150mM KOAc, 5mM $Mg(OAc)_2$, 2 mM PMSF and protease inhibitor cocktail) and overlayered on top of a 2 step sucrose density gradient (1.2 M and 1.5 M sucrose in 20mM HEPES, pH

7.4, 50 mM KOAc, 2 mM EDTA, 2 mM PMSF and protease inhibitor). Gradients were subjected to centrifugation at 35,000 rpm for 1 hr at 4°C (Beckman SW41) and the bulk ER fraction was collected at the 1.2/1.5 M interface.

Fluorescence microscopy

Fluorescent images were acquired on either an Axioskop 2 microscope with 100x/1.4 Plan-Apochromat objective (Zeiss, Thornwood, NY) and an Orca-ER cooled CCD camera (Hamamatsu) running NIS Elements 4.20 Lambda (Nikon, Melville, NY), AxioObserver.Z1 microscope equipped with a Colibri LED excitation source with an Orca ER camera running Axiovision acquisition software (Zeiss, Thornwood, NY), a Nikon A1R MP confocal microscope with an Evolve EMCCD (Photometrics, Tuscon, AZ) camera and 100x/1.45 CFI Plan Apo Lambda objective running NIS Elements 4.20 (Nikon, Melville, NY), or Nikon eclipse Ti with an Evolve EMCCD (Photometrics, Tuscon, AZ) camera and 100x 1.45 CFI Apo TIRF objective running NIS Elements (Nikon, Melville, NY). Fluorescent channels were acquired using (482/28ex and 525/36em) for GFP, (572/35ex and 632/60em) for mCherry, (350/15ex and 460/50em) for DAPI and MDH, roGFP as described in (Vevea et al., 2013), and Nile red using the GFP and mCherry channels. Unless otherwise noted, Z-stacks were acquired using 0.5 micron Z spacing and a total of 13 slices (6 microns). Samples were grown to mid-log phase and concentrated in a tabletop centrifuge, and 2 µL were placed on glass slides and covered with a #1.5 coverslip. For extended time-lapse imaging (>15 min), cells were loaded into a CellASIC (EMD Millipore, Billerica, MA) Y04 imaging plate. Cells were loaded and perfused with SC media at 2.0 psi for the duration of the experiment. All images and image series were imported into Volocity libraries (Perkin Elmer, Waltham, MA) for deconvolution and quantitation.

Image Quantitation

Organelle Aggregation: During normal cell cycles, mitochondria and ER do not aggregate in cytosolic clusters. The time that organelle aggregation occurred after removal of choline from the media in WT and *cho2*Δ strains was determined by visual inspection of cells expressing organelle targeted fluorescent proteins and time-lapse imaging.

Organelle Distribution: Distribution of mitochondria and ER was analyzed as sum fluorescence in the mother or bud relative to total organelle fluorescence of the budding pair. Deconvolved, fluorescent channels were thresholded and analyzed for integrated intensity in ROIs outlining the mother, bud, or budding pair. All measurements and calculations were imported and performed in Microsoft Excel (Seattle, WA).

Total Mitochondrial Motility: Mitochondrial motility was assayed on a method described by (De Vos and Sheetz, 2007). Mitochondria were imaged using Cit1p-mCherry, collected as 6 µm Z-stacks with 1 µm Z-spacing, and acquired every 30 sec for 7.5 min. Z-stacks were deconvolved in Volocity and exported to ImageJ (NIH). Stacks were compressed to a hyperstack using the "Stack to Hyperstack" command and made into maximum projections using the "Z Project" command. Contrast was automatically enhanced using the "Enhance Contrast" command and registry corrected using the "StackReg" command. Images were then thresholded manually and the background was changed to "not a number" (NaN) using the "NaN Background" command. Stacks were made into binary images using the "Make Binary" command and the "Total Motility" plugin was run to generate the percent motile mitochondria. Results were copied to Microsoft Excel (Seattle, WA), and each time point was subtracted from the previous (n+1)-(n) to obtain the number of pixels that had changed positions (during mitochondrial movement). To calculate the percentage of mitochondrial motility, the number of pixels that changed position was divided by the total number of pixels. All results were averaged for each strain and represented in a histogram bar graph as the mean +/- SEM.

Mitochondrial Redox: Mitochondrial redox was assayed as described in (Vevea et al., 2013).

The Velocity of Mitochondrial Movement: Mitochondria were imaged using Cit1p-mCherry, collected as 6 µm Z-stacks with 1 µm Z-spacing, acquired every sec for 1 min. Z-stacks were deconvolved in using Volocity software (Perkin Elmer, Inc., Waltham MA). Directed events were defined as those that exhibited linear movement for 3 consecutive time points. The velocity was measured as a change in the position of a moving mitochondrion as a function of time.

Multibudded Cell Analysis: Multibudded cells were defined as cells with 2 or more buds. The numbers of multibudded cells were compared to total number of single budded cells to obtain percentage of budded cell that were multibudded.

UPR Organelle Aggregation Assay: Aggregates of ER and mitochondria were defined as organelle clumps, typically in the vicinity of the nucleus. Numbers of affected cells were compared to total number of cells (single and budding cells).

MDH Fluorescence: Raw images (non-deconvolved), were assayed for total MDH fluorescence. ROI were drawn around budding cells and the MDH channel was thresholded and analyzed for integrated intensity. Results were imported to and quantified in Microsoft Excel (Seattle, WA).

Analysis of GFP-Atg8p-labeled PAS: Z-stacks of yeast cells expressing GFP-Atg8p were recorded and deconvolved in Volocity software (Perkin Elmer, Inc., Waltham MA). Budding cells were analyzed for punctate or circular structures representing PAS and autophagosomes respectively. These structures were manually counted on a cell-by-cell basis in Volocity and recorded in Microsoft Excel (Seattle, WA).

Other methods

Yeast cells were transformed using the lithium acetate method (Longtine et al., 1998). All chemicals and materials were obtained from Sigma-Aldrich (St. Louis, MO) unless otherwise noted.

Yeast Strains Used in this Study

Strain	Genotype	Primer set
BY4741	*MAT**a** his3Δ0 leu2Δ0 met15Δ0 ura3Δ0*	Open Biosystems (Huntsville, AL)
JVY002	*MAT**a**: pmito-roGFP$_1$:URA3*	McFaline-Figueroa and Vevea et al 2011
JVY063	*MAT**a**: CIT1-yEpolylinker-mCherry::hphMX4 PHO88-GFP(S65T)::KanMX*	pCY CIT1, pFa6 PHO88
JVY064	*MAT**a**: cho2Δ::LEU2 CIT1-yEpolylinker-mCherry::hphMX4 PHO88-GFP(S65T)::KanMX*	pOMΔ CHO2, pCY CIT1, pFa6 PHO88
JVY065	*MAT**a**: cho2Δ::LEU2 [pmito-roGFP$_1$:URA3]*	pOMΔ CHO2
JVY075	*MAT**a**: ylr312cΔ::URA3 CIT1-yEpolylinker-mCherry::hphMX4 PHO88-GFP(S65T)::KanMX*	pOMΔ YLR312c, pCY CIT1, pFa6 PHO88
JVY076	*MAT**a**: cho2Δ::LEU2 ylr312cΔ::URA3 CIT1-yEpolylinker-mCherry::hphMX4 PHO88-GFP(S65T)::KanMX*	pOMΔ CHO2, pOMΔ YLR312c, pCY CIT1, pFa6 PHO88
JVY084	*MAT**a**: YLR312c-GFP(S65T)::KanMX*	pFa6 YLR312c
JVY087	*MAT**a**: CIT1-yEpolylinker-mCherry::hphMX4 PHO88-GFP(S65T)::KanMX [p413GALYLR312c:HIS3]*	pCY CIT1, pFa6 PHO88, YLR312c OE
JVY105	*MAT**a**: GFP-lox-ATG8*	pOM GFP-ATG8
JVY106	*MAT**a**: ylr312c Δ::LEU2 GFP(S65T)-lox-ATG8*	pOM GFP-ATG8, pOMΔ YLR312c,
JVY109	*MAT**a**: GFP(S65T)-lox-ATG8 ATG9-yEpolylinker-mCherry::hphMX4*	pOM GFP-ATG8, pCY ATG9
JVY110	*MAT**a**: YLR312c-GFP(S65T)::KanMX [p413GALYLR312c-GFP(S65T):HIS3]*	pFa6 YLR312c, YLR312c-GFP OE
JVY120	*MAT**a**: YLR312c-GFP(S65T)::KanMX PHO88-yEpolylinker-mCherry::hphMX4*	pFa6 YLR312c, pCY PHO88
JVY124	*MAT**a**: cho2Δ::LEU2 GFP(S65T)-loxed-ATG8 ATG9-yEpolylinker-mCherry::hphMX4*	pOMΔ CHO2, pOM GFP-ATG8, pCY ATG9
JVY125	*MAT**a**: atg7Δ::URA3 CIT1-yEpolylinker-mCherry::hphMX4 PHO88-GFP(S65T)::KanMX*	pOMΔ ATG7, pCY CIT1, pFa6 PHO88
JVY126	*MAT**a**: cho2Δ::LEU2 atg7Δ::URA3 CIT1-yEpolylinker-mCherry::hphMX4 PHO88-GFP(S65T)::KanMX*	pOMΔ CHO2, pOMΔ ATG7, pCY CIT1, pFa6 PHO88
JVY136	*MAT**a**: PHO88-GFP(S65T)::KanMX ERG6-yEpolylinker-mCherry::hphMX4*	pFa6 PHO88, pCY ERG6
JVY137	*MAT**a**: cho2Δ::LEU2 PHO88-GFP(S65T)::KanMX ERG6-yEpolylinker-mCherry::hphMX4*	pOMΔ CHO2, pFa6 PHO88, pCY ERG6
JVY141	*MAT**a**: GFP(S65T)-lox-ATG8 CIT1-yEpolylinker-mCherry::hphMX4*	pOM GFP-ATG8, pCY CIT1
JVY142	*MAT**a**: GFP(S65T)-lox-ATG8 PHO88-yEpolylinker-mCherry::hphMX4*	pOM GFP-ATG8,

		pCY PHO88
JVY143	*MAT**a**: GFP(S65T)-lox-ATG8 ERG6-yEpolylinker-mCherry::hphMX4*	pOM GFP-ATG8, pCY ERG6
JVY144	*MAT**a**: cho2Δ::LEU2 GFP(S65T)-lox-ATG8 CIT1-yEpolylinker-mCherry::hphMX4*	pOMΔ CHO2, pOM GFP-ATG8, pCY CIT1
JVY145	*MAT**a**: cho2Δ::LEU2 GFP-lox-ATG8 PHO88-yEpolylinker-mCherry::hphMX4*	pOMΔ CHO2, pOM GFP-ATG8, pCY PHO88
JVY146	*MAT**a**: cho2Δ::LEU2 GFP(S65T)-lox-ATG8 ERG6-yEpolylinker-mCherry::hphMX4*	pOMΔ CHO2, pOM GFP-ATG8, pCY ERG6
JVY147	*MAT**a**: ylr312c Δ::LEU2 GFP(S65T)-lox-ATG8 ERG6-yEpolylinker-mCherry::hphMX4*	pOMΔ YLR312c, pOM GFP-ATG8, pCY ERG6
JVY152	*MAT**a**: cho2Δ::LEU2 lro1Δ::LOX dga1Δ::URA3 CIT1-yEpolylinker-mCherry::hphMX4 PHO88-GFP(S65T)::KanMX*	pCY CIT1, pFa6 PHO88, pOMΔ CHO2, pOMΔ LRO1, pOMΔ DGA1,
JVY153	*MAT**a**: dga1Δ::LEU2 lro1Δ::URA3 CIT1-yEpolylinker-mCherry::hphMX4 PHO88-GFP(S65T)::KanMX*	pCY CIT1, pFa6 PHO88, pOMΔ LRO1, pOMΔ DGA1,
JVY160	*MAT**a**: HSP104-yEpolylinker-mCherry::hphMX4 PHO88-GFP(S65T)::KanMX*	pCY HSP104, pFa6 PHO88
JVY162	*MAT**a**: cho2Δ::LEU2 HSP104-yEpolylinker-mCherry::hphMX4 PHO88-GFP(S65T)::KanMX*	pOMΔ CHO2, pCY HSP104, pCY PHO88
JVY178	*MAT**a**: cho2Δ::LEU2 atg7Δ::URA3 GFP(S65T)-lox-ATG8 ERG6-yEpolylinker-mCherry::hphMX4*	pOMΔ CHO2, pOMΔ ATG7, pOM GFP-ATG8, pCY ERG6
JVY179	*MAT**a**: cho2Δ::LEU2 pep4Δ::URA3 GFP(S65T)-lox-ATG8 ERG6-yEpolylinker-mCherry::hphMX4*	pOMΔ CHO2, pOMΔ PEP4, pOM GFP-ATG8, pCY ERG6
JVY180	*MAT**a**: cho2Δ::LEU2 vps4Δ::URA3 GFP(S65T)-lox-ATG8 ERG6-yEpolylinker-mCherry::hphMX4*	pOMΔ CHO2, pOMΔ VPS4, pOM GFP-ATG8, pCY ERG6

Primers Used in this Study

Primer pair name	Forward	Reverse
pCY CIT1	ACCGAAAAATACAAGGAGTTGGTAAAGAAAATCGAAAGTAAGAACGGTGACGGTGCTGGTTTA	ATAAACTACTCATTCGTATATGAAAATACGTGTTTGAATAGTCGCATCGATGAATTCGAGCTCG
pFa6 PHO88	AGAAGCTGAAAGAGCCGGTAACGCTGGTGTTAAGGCTGAACGGATCCCCGGGTTAATTAA	AAAACTAGGAAAAAAAAATACTTCGCTTTTGATCGAATCAGAATTCGAGCTCGTTTAAAC
pOMΔ CHO2	CCGCCCTGAATATTTCGAGTGATTTTCTTAGTGACAAAGCTGCAGGTCGACAACCCTTAAT	TAACTACTTCTATTCAAAATGTTAACTTGAATCCTAGTACGCAGCGTACGGATATCACCTA
pOM GFP-ATG8	TAATTGTAAAGTTGAGAAAATCATAATAAAATAATTACTAGAGACATGTGCAGGTCGACAACCCTTAAT	CGCCTTCCTTTTTTCAAATGGATATTCAGACTTAAATGTAGACTTGCGGCCGCATAGGCCACT
pCY ATG9	TTAGGACTTGTTAAAGAGTATTACAAGAAGTCTGACGTCGGAAGAGGTGACGGTGCTGGTTTA	GAATAATATATGCATTTAGGTAAATACGAAAAAGAAAGGAAACAGATCGATGAATTCGAGCTCG
pOMΔ ATG7	GATAACTAAAGTTCATTATATTTCAACAAATATAAGATAATCAAGTGCAGGTCGACAACCCTTAAT	ATTACGGAAAGTGGCACCACAATATGTACCAATGCTATTATATGCGCAGCGTACGGATATCACCTA
pCY ERG6	GAAAACGCCGAAACCCCCTCCCAAACTTCCCAAGAAGCAACTCAAGGTGACGGTGCTGGTTTA	ATCTGCATATATAGGAAAATAGGTATATATCGTGCGCTTTATTTGATCGATGAATTCGAGCTCG
pCY PHO88	AGAAGCTGAAAGAGCCGGTAACGCTGGTGTTAAGGCTGAAGGTGACGGTGCTGGTTTA	AAAACTAGGAAAAAAAAATACTTCGCTTTTGATCGAATCAATCGATGAATTCGAGCTCG
pOMΔ LRO1	GCCATTACAAAAGGTTCTCTACCAACGAATTCGGCGACAATCGAGTGCAGGTCGACAACCCTTAAT	CTTTTCGCTCTTTGAAATAATACACGGATGGATAGTGAGTCAATGGCAGCGTACGGATATCACCTA
pOMΔ DGA1	ACATATACATAAGGAAACGCAGAGGCATACAGTTTGAACAGTCACTGCAGGTCGACAACCCTTAAT	AAATCCTTATTTATTCTAACATATTTTGTGTTTTCCAATGAATTCGCAGCGTACGGATATCACCTA
pOMΔ YLR312c	CATCATGCTATTTTCCATGTTTCCGAGCTTGTCTACTCTTTGCAGGTCGACAACCCTTAAT	TTCTTTTGTTAATTTCATTCTTCATGCTGGGTTTTGGATGGCAGCGTACGGATATCACCTA
YLR312c OE	GCGCACTAGTATGTCAGAAGAAGACGATCATTGG	GCGCCTCGAGCTAGTGTTTGCACTTAAAATAATTTTTTTTC
YLR312c-GFP OE	GCGCACTAGTATGTCAGAAGAAGACGATCATTGG	CCGGCTCGAGCTATTTGTATAGTTCATCCATGCCATGTG
pFa6 YLR312c	GTCAGAATGCAGGAAAAAAAATTATTTTAAGTGCAAACACCGGATCCCCGGGTTAATTAA	ATTTAAAGGAGGGATATATGACACTCCTACTAAGCAGTCGGAATTCGAGCTCGTTTAAAC
pCY YLR312c	GTCAGAATGCAGGAAAAAAAATTATTTTAAGTGCAAACACGGTGACGGTGCTGGTTTA	ATTTAAAGGAGGGATATATGACACTCCTACTAAGCAGTCGATCGATGAATTCGAGCTCG
pCY HSP104	CGATAATGAGGACAGTATGGAAATTGATGATGACCTAGATGGTGACGGTGCTGGTTTA	TATTATATTACTGATTCTTGTTCGAAAGTTTTTAAAAATCATCGATGAATTCGAGCTCG
pOM PEP4	CTAGTATTTAATCCAAATAAAATTCAAACAAAAACCAAAACTAACTGCAGGTCGACAACCCTTAAT	TAGATGGCAGAAAAGGATAGGGCGGAGAAGTAAGAAAAGTTTAGCGCAGCGTACGGATATCACCTA
pOM VPS4	GGAAGACAAAAATAAAGCAGCATAGAGTGCCTATAGTAGATGGGGTGCAGGTCGACAACCCTTAAT	TTTTTATTTTCATGTACACAAGAAATCTACATTAGCACGTTAATCGCAGCGTACGGATATCACCT

Supplemental References

Bligh, E.G., and Dyer, W.J. (1959). A rapid method of total lipid extraction and purification. Can J Biochem Physiol *37*, 911-917.

De Vos, K.J., and Sheetz, M.P. (2007). Visualization and quantification of mitochondrial dynamics in living animal cells. Methods in cell biology *80*, 627-682.

Gauss, R., Trautwein, M., Sommer, T., and Spang, A. (2005). New modules for the repeated internal and N-terminal epitope tagging of genes in Saccharomyces cerevisiae. Yeast (Chichester, England) *22*, 1-12.

Huang, D.W., Sherman, B.T., and Lempicki, R.a. (2009). Systematic and integrative analysis of large gene lists using DAVID bioinformatics resources. Nature protocols *4*, 44-57.

Ladner, C.L., Yang, J., Turner, R.J., and Edwards, R.a. (2004). Visible fluorescent detection of proteins in polyacrylamide gels without staining. Analytical biochemistry *326*, 13-20.

Longtine, M.S., McKenzie, a., Demarini, D.J., Shah, N.G., Wach, a., Brachat, a., Philippsen, P., and Pringle, J.R. (1998). Additional modules for versatile and economical PCR-based gene deletion and modification in Saccharomyces cerevisiae. Yeast (Chichester, England) *14*, 953-961.

Perkins, E.M., and McCaffery, J.M. (2007). Conventional and immunoelectron microscopy of mitochondria. Methods in molecular biology *372*, 467-483.

Schmidt, C., Ploier, B., Koch, B., and Daum, G. (2013). Analysis of yeast lipid droplet proteome and lipidome. Methods Cell Biol *116*, 15-37.

Supek, F., Bošnjak, M., Škunca, N., and Šmuc, T. (2011). REVIGO summarizes and visualizes long lists of gene ontology terms. PloS one *6*, e21800-e21800.

Trapnell, C., Roberts, A., Goff, L., Pertea, G., Kim, D., Kelley, D.R., Pimentel, H., Salzberg, S.L., Rinn, J.L., and Pachter, L. (2012). Differential gene and transcript expression analysis of RNA-seq experiments with TopHat and Cufflinks. Nature Protocols *7*, 562-578.

Vevea, J.D., Wolken, D.M., Swayne, T.C., White, A.B., and Pon, L.A. (2013). Ratiometric biosensors that measure mitochondrial redox state and ATP in living yeast cells. Journal of visualized experiments : JoVE.

Wuestehube, L.J., and Schekman, R.W. (1992). Reconstitution of transport from endoplasmic reticulum to Golgi complex using endoplasmic reticulum-enriched membrane fraction from yeast. Methods Enzymol *219*, 124-136.

Young, C.L., Raden, D.L., and Caplan, J.L. (2012). Cassette series designed for live-cell imaging of proteins and high-resolution techniques in yeast. Yeast, 119-136.